The α-Terpineol to 1,8-Cineole Cyclization Reaction of Tobacco Terpene Synthases[1]

Birgit Piechulla*, Richard Bartelt[2], Anne Brosemann[2], Uta Effmert, Harro Bouwmeester, Frank Hippauf[2], and Wolfgang Brandt

Institute of Biological Sciences, Biochemistry, University of Rostock, 18059 Rostock, Germany (B.P., A.B., U.E., F.H.); Leibniz Institute of Plant Biochemistry, 06120 Halle (Saale), Germany (R.B., W.B.); and Plant Sciences, University of Wageningen, 6708PB Wageningen, The Netherlands (H.B.)

ORCID IDs: 0000-0002-2744-6796 (U.E.); 0000-0002-0825-1491 (W.B.).

Flowers of *Nicotiana* species emit a characteristic blend including the cineole cassette monoterpenes. This set of terpenes is synthesized by multiproduct enzymes, with either 1,8-cineole or α-terpineol contributing most to the volatile spectrum, thus referring to cineole or terpineol synthase, respectively. To understand the molecular and structural requirements of the enzymes that favor the biochemical formation of α-terpineol and 1,8-cineole, site-directed mutagenesis, in silico modeling, and semiempiric calculations were performed. Our results indicate the formation of α-terpineol by a nucleophilic attack of water. During this attack, the α-terpinyl cation is stabilized by π-stacking with a tryptophan side chain (tryptophan-253). The hypothesized catalytic mechanism of α-terpineol-to-1,8-cineole conversion is initiated by a catalytic dyad (histidine-502 and glutamate-249), acting as a base, and a threonine (threonine-278) providing the subsequent rearrangement from terpineol to cineol by catalyzing the autoprotonation of (*S*)-(−)-α-terpineol, which is the favored enantiomer product of the recombinant enzymes. Furthermore, by site-directed mutagenesis, we were able to identify amino acids at positions 147, 148, and 266 that determine the different terpineol-cineole ratios in *Nicotiana suaveolens* cineole synthase and *Nicotiana langsdorffii* terpineol synthase. Since amino acid 266 is more than 10 Å away from the active site, an indirect effect of this amino acid exchange on the catalysis is discussed.

Monoterpenes are a large group of natural products often found in essential oils and defensive oleoresins of plants (Bohlmann and Keeling, 2008). They consist of a 10-carbon skeleton and can be divided into acyclic, monocyclic, and bicyclic monoterpenes (Degenhardt et al., 2009; Fähnrich et al., 2011). They often represent the majority in floral scent bouquets of seed plants, but other plant organs (e.g. leaves and roots) also release them into the atmosphere or rhizosphere. Monoterpenes have different biological functions: they serve as attractants and guides for pollinators and as defense compounds to protect plants against herbivores, and they act as intraspecific and interspecific plant communication molecules (Gershenzon and Dudareva, 2007).

The biosynthesis of monoterpenes starts with the cleavage of the phosphoester bond of the common substrate geranyl diphosphate (GPP). The fate of the resulting geranyl cation determines the nature of the final product (Degenhardt et al., 2009; Fig. 1). While acyclic monoterpenes are direct products of the acyclic geranyl or linalyl cation, all cyclic monoterpenes share one additional precursor, the α-terpinyl cation, which is formed by an intramolecular electrophilic addition of the cation to the double bond at C6. Recent evidence indicates that the direct isomerization of a geranyl cation to the cisoid-isomer, which was so far considered unlikely, is feasible (Zhang and Tiefenbacher, 2015). The α-terpinyl cation can now undergo further intramolecular additions, rearrangements, and hydride shifts, leading to a broad structural variety of carbocations. Quenching of these cations by either attack of a nucleophile or deprotonation then leads to the final monoterpene products. The synthesis of 1,8-cineole is reported via α-terpineol (Degenhardt et al., 2009), but the molecular details underlying the reaction mechanism to 1,8-cineole remain elusive. It is known that the double bond of α-terpineol is protonated and that this results in an intermediate, which is the precursor for the cyclization to 1,8-cineole (Wise et al., 2002). However, α-terpineol cannot be converted in cell-free extracts (Croteau et al., 1994), and it is also hypothesized that a pathway independent from α-terpineol might exist.

Within the genus *Nicotiana*, several species emit a characteristic floral monoterpene volatile pattern consisting of 1,8-cineole, β-myrcene, limonene, sabinene, α-/β-pinene, and α-terpineol. As 1,8-cineole represents the main component of the scent mixture, this set of compounds was named the cineole cassette (Raguso et al., 2006). Until now, cineole cassette monoterpene synthases were isolated from seven *Nicotiana* spp. It was shown that for *Nicotiana*

[1] This work was supported by the University of Rostock, the Institute for Plant Biochemistry (Halle), and the Deutsche Forschungsgemeinschaft (grant no. Pi 153/22).

[2] These authors contributed equally to the article.

* Address correspondence to birgit.piechulla@uni-rostock.de.

The author responsible for distribution of materials integral to the findings presented in this article in accordance with the policy described in the Instructions for Authors (www.plantphysiol.org) is: Birgit Piechulla (birgit.piechulla@uni-rostock.de).

B.P. and W.B. designed the research; F.H., A.B., R.B., U.E., and H.B. performed the research; F.H., A.B., R.B., U.E., B.P., and H.B. analyzed the data; R.B. and F.H prepared the article drafts; B.P. finalized the article.

www.plantphysiol.org/cgi/doi/10.1104/pp.16.01378

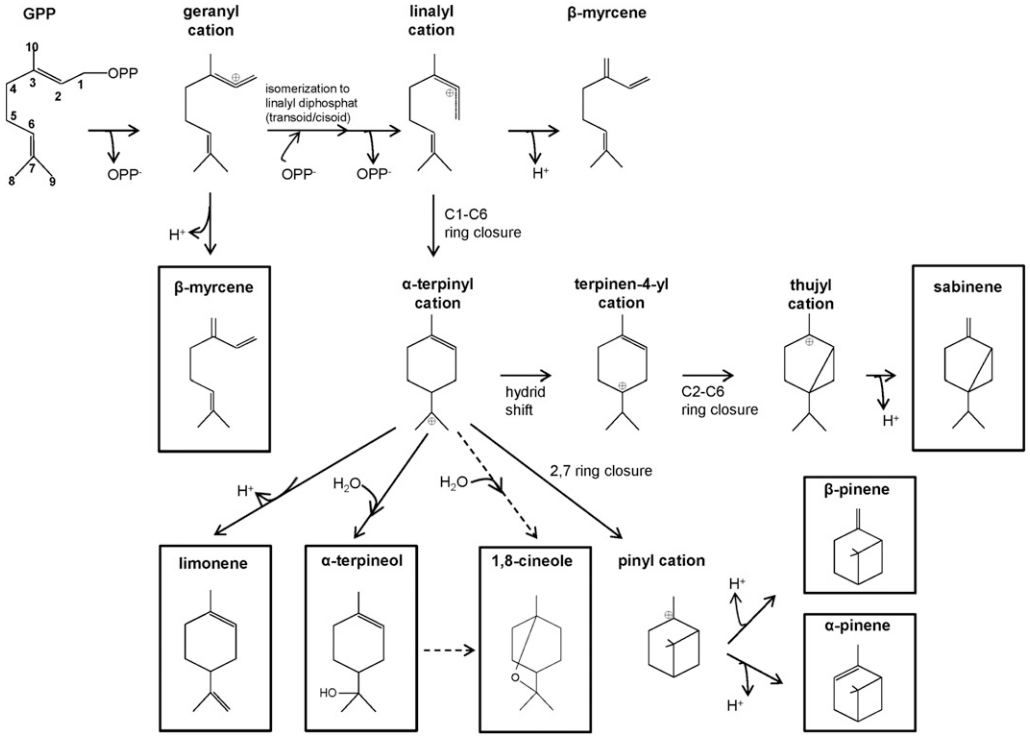

Figure 1. Synthesis of cineole cassette monoterpenes. The substrate GPP is ionized by diphosphate elimination, resulting in the geranyl cation. Subsequently, this cation is converted into the linalyl cation and α-terpinyl cation. The synthesis of the acyclic β-myrcene might proceed via the geranyl cation or via the linalyl cation by deprotonation. The intermediate α-terpinyl cation is the precursor for all cyclic monoterpenes. The 2,7-ring closure results in the pinyl cation, which is deprotonated to synthesize β-pinene and α-pinene. Sabinene, with a cyclopropane ring, is released after two carbocation formations and 2,6-ring closure. α-Terpineol is formed after water capture of the α-terpinyl cation. Broken lines indicate possible reactions leading to 1,8-cineole. A cyclization reaction resulting in 1,8-cineole uses α-terpineol as a precursor (modified from Degenhardt et al. [2009]).

bonariensis, *Nicotiana forgetiana*, *Nicotiana longiflora*, *Nicotiana suaveolens*, and *Nicotiana noctiflora*, the cineole cassette monoterpenes were indeed synthesized by just one enzyme, which was called cineole synthase (CIN; Fähnrich et al., 2011, 2012, 2014). The corresponding enzymes of *Nicotiana alata* and *Nicotiana langsdorffii*, however, released α-terpineol as the main compound and were subsequently named terpineol synthases (TERs; Fähnrich et al., 2012). All *Nicotiana* spp. cineole cassette monoterpene synthases possess sequence similarities and share conserved motifs (Fig. 2). At the N-terminal end of the protein sequence is a transit peptide that is essential for transport into the plastids (Turner et al., 1999). The first motif of the mature protein sequence is $RR(X)_8W$. It plays a role in isomerization of the substrate (Williams et al., 1998). The motifs RWW and CYMNE have been identified in all CINs and TERs of *Nicotiana* spp., but the functions of these motifs remain elusive. The RDR motif is involved in the protection of the carbocation intermediate against nucleophilic attack (Starks et al., 1997). Mutant analyses and crystallization of monoterpene synthases from *Salvia* spp. have demonstrated that the NALV motif is responsible for the product outcome and enzyme specificity. The Asp-rich DDXXD motif and the NSE/DTE motif play important roles in the coordination and binding of divalent metal ions to form the trinuclear magnesium cluster, which supports substrate ionization, followed by the cyclization reaction to the α-terpinyl cation (Christianson, 2006).

Despite these conserved motifs and sequence similarities, there are considerable differences in the product composition regarding the α-terpineol-to-cineole ratio. Consequently, in our work, we wanted to unravel structural features of *Nicotiana* spp. cineole cassette monoterpene synthases, which control this ratio of the main products. To reach this goal, we wanted to establish and verify a putative mechanism of the enzymatic formation of α-terpineol and cineole.

RESULTS

Site-Directed Mutagenesis Based on Sequence Analysis of *Nicotiana* spp. Cineole Cassette Monoterpene Synthases

Sequence comparison of all identified *Nicotiana* spp. cineole cassette monoterpene synthases (Fähnrich et al., 2011, 2012, 2014) revealed sequence identities of 89% to 99% corresponding to one to 53 amino acid alterations (Supplemental Table S1). To identify sequence features

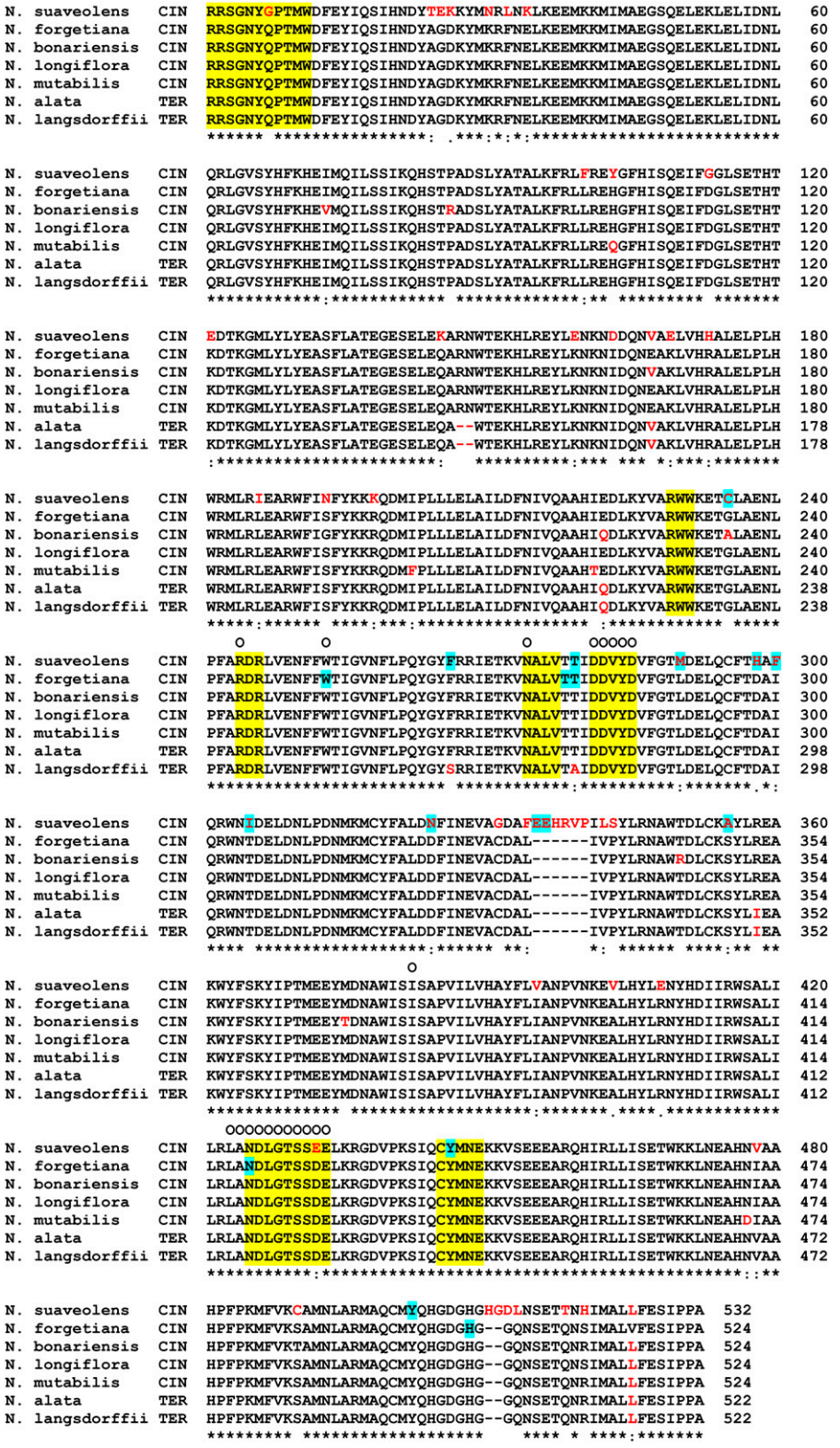

Figure 2. Amino acid sequence alignment of the cineole and terpineol synthases of seven *Nicotiana* spp. Amino acid sequence alignment is shown for the cineole synthases of *N. suaveolens*, *N. forgetiana*, *N. bonariensis*, *N. longiflora*, and *N. mutabilis* and the terpineol synthases of *N. alata* and *N. langsdorffii*. Sequences of putative mature enzymes were aligned using ClustalW 2.0.10 (Thompson et al., 1994). Conserved sequence motifs of monoterpene synthases are highlighted in yellow. Black circles above the sequence indicate amino acids of the active pocket of monoterpene synthase according to Fähnrich et al. (2012). Asterisks, Identical amino acids; spaces, different amino acids; double dots, amino acids that differ from each other but have similar properties; single dots, amino acids that differ from each other but have few similar properties (EMBL-EBI, 2014). Red letters, Amino acid differences compared with the sequence of *N. forgetiana*; cyan highlights, amino acid mutations reported in this article. Mutated residues and sequence motifs correspond to Figure 4, B and C.

discriminating between the identified five CIN and two TER enzymes, sequences were analyzed in more detail. Twenty amino acids were assumed to be involved in the formation of the active pocket, Arg-244, Trp-253, Asn-274, Asp-281 to Asp-285, Ile-376, and Leu-417 to Asp-426 (numbering according to the sequence of *N. forgetiana* [Fig. 2]; summarized in Fähnrich et al., 2012). These residues are conserved in all sequences

except the *N. suaveolens* CIN, where Asp-426 is replaced by Glu. Therefore, we concluded that amino acids outside of the active pocket must influence the terpineol and cineole synthesis. Subsequently, amino acid differences of two TER and five CIN enzymes were summarized and analyzed (Supplemental Table S2; amino acid numbers correspond to the *N. forgetiana* sequence; Fähnrich et al., 2014). Remarkable differences include the amino acids Arg-147 and Asn-148, which are missing in the TERs of *N. alata* and *N. langsdorffii*, and Arg-352, which is conserved in all CINs and changed into an Ile in the TERs. The amino acids Arg-147 and Asn-148 were inserted into the *N. langsdorffii* TER, but both had only a small impact on cineole synthesis (Fig. 3C). The residue Arg-352 lies on the surface of the outermost helix of the C-terminal domain, more than 10 Å away from the active pocket. Because of this location, it was concluded that it may not influence the terpineol-cineole ratio. In addition, some semiconserved amino acids appear at positions 167, 222, and 472, where three or four of five CINs share a common amino acid, while amino acids of both TERs are different, but these positions also did not convincingly influence the terpineol-cineole ratio. Consequently, the multiple sequence alignment approach alone did not highlight possible candidate amino acids. Therefore, a one-to-one comparison approach supported by in silico modeling was used.

Site-Directed Mutagenesis Based on Sequence Comparison of *N. suaveolens* CIN and *N. langsdorffii* TER

In order to unravel the origin of the structural differences that discriminate between 1,8-cineole or α-terpineol synthesis, site-directed mutagenesis of *N. suaveolens* CIN was performed. Sequence alignment of the CIN of *N. suaveolens* and TER of *N. langsdorffii* (Fig. 2; Supplemental Table S1; sequence identity, 89%) and three-dimensional (3D) modeling (Fig. 4C) were used to select amino acids (Supplemental Table S3) for a mutational screen. We hypothesized that mutations close to the active pocket or conserved motifs disturb the proposed functions of these motifs and the enzyme. Additionally, we mutated amino acids that we suspected to be involved in the enzymatic catalysis. The amino acids at respective sites of the *N. suaveolens* CIN were altered and changed into the residues found at the equivalent positions in the *N. langsdorffii* TER sequence (Fig. 2, highlighted in cyan; Supplemental Table S2). The product profiles of the mutated enzymes were obtained from crude extracts of *Escherichia coli* (Supplemental Fig. S1, A–G), and the results are summarized in Supplemental Table S4. Although the distributions of the five detectable products sabinene, β-myrcene, limonene, 1,8-cineole, and α-terpineol changed slightly in all these mutants, none of them shifted the product spectrum significantly toward α-terpineol. The only exception represented the mutation at position 266 (F266S). Therefore, this amino acid position was investigated in more detail in the mutants F266T, F266V, F266Y, and F266C. Respective amino acid alterations were selected to test (1) aromatic versus nonaromatic/bulky versus less unwieldy amino acids with hydroxyl groups, (2) amino acids with potential other hydrogen bond residues, or (3) amino acids without bulky and hydrophobic side chains. The purified proteins of three mutants (Supplemental Fig. S2) showed decreases of the K_m values of F266T (0.04 μM) and F266V (0.04 μM) compared with the wild-type enzyme (0.19 μM) and the F266S mutant (0.12 μM; Table I). The k_{cat} of F266T and F266V is 1 order of magnitude lower compared with the wild-type enzyme and with F266S ($2.9–4 \times 10^{-4}$ s^{-1}). The catalytic efficiencies (k_{cat}/K_m) of the wild-type and mutant enzymes were approximately the same and in the range of other plant cineole synthases (Supplemental Table S12). The examination of the product composition of purified enzymes resembled that of the corresponding crude extracts. These mutations produced similar amounts of α-terpineol compared with the wild-type enzyme in similar terpineol:cineole ratios close to 1:1, while the wild-type ratio was 1:2.4 (Fig. 3B; Supplemental Tables S5–S7). Again, only *N. suaveolens* F266S produced more α-terpineol than cineole; thus, this mutated enzyme changed from a CIN to a TER according to the classification.

Further support for the importance of the Phe-266 position for 1,8-cineol synthesis was provided by a reverse mutation in the TER of *N. langsdorffii*, where Ser (Ser-264) is present in the wild-type enzyme (Fig. 2; Supplemental Table S2). This mutant, S264F, produced twice as much 1,8-cineole as α-terpineol (Fig. 3C), indicating that the TER enzyme was converted into a CIN. Interestingly, other mutations based on sequence differences between *N. langsdorffii* TER and *N. suaveolens* CIN enzymes, such as A277T and Q220E, did not alter the product profiles or the 1,8-cineole-to-α-terpineol ratio (Supplemental Fig. S3), while the insertion of the Arg-147/Asn-148 combination with A277T increased 1,8-cineole levels compared with the wild-type TER (Fig. 3C), again indicating that distantly located amino acids influence the reaction mechanism in the active site.

In Silico Investigations and Site-Directed Mutagenesis of *N. forgetiana* CIN

Despite a sequence identity of 98% between *N. langsdorffii* TER and *N. forgetiana* CIN (Supplemental Table S1), both enzymes differ considerably in their main products and terpineol-cineole ratios (Fähnrich et al., 2011, 2012; Fig. 3). Therefore, the mechanism of product formation of the *N. forgetiana* CIN was investigated by in silico investigations, and the putative reaction mechanism was verified by site-directed mutagenesis and in vitro assays with purified enzymes. The wild-type enzyme of *N. forgetiana* CIN synthesized α-pinene, β-pinene, sabinene, β-myrcene, limonene, α-terpineol, and 1,8-cineole (Fig. 3; Supplemental Tables S8–S10; Supplemental Fig. S4). This volatile

A ***Nicotiana forgetiana***

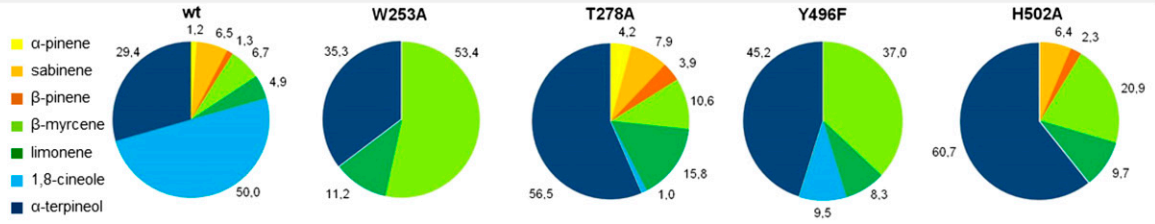

Specific activity [pkat/mg]					
α-pinene	3.38	0.00	2.03	0.00	0.00
sabinene	18.40	0.00	3.77	0.00	1.13
β-pinene	3.68	0.00	1.89	0.00	0.41
β-myrcene	19.10	3.74	5.08	2.16	3.69
limonene	13.95	0.79	7.54	0.49	1.72
1,8-cineole	125.52	0.00	0.43	0.49	0.00
α-terpineol	73.92	2.19	23.89	2.33	9.47
Total specific activity [pkat/mg]	257.94	6.72	44.61	5.46	16.41
α-terpineol/1,8-cineole ratio	1 : 1.7	1 : 0	1 : 0.02	1 : 0.2	1 : 0

B ***Nicotiana suaveolens***

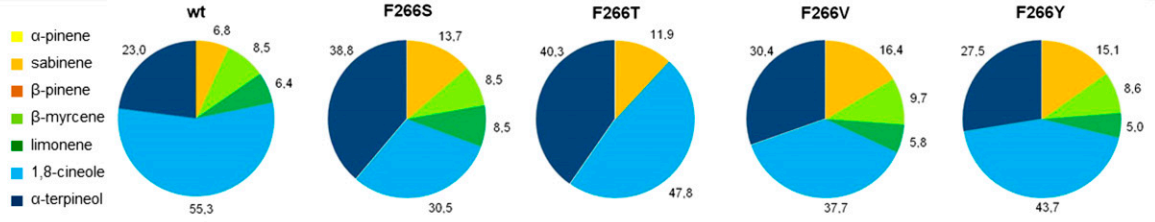

Specific activity [pkat/mg]					
α-pinene	0.00	0.00	0.00	0.00	0.00
sabinene	5.48	6.05	1.94	8.97	7.00
β-pinene	0.00	0.00	0.00	0.00	0.00
β-myrcene	5.85	3.78	0.00	5.31	3.99
limonene	5.26	3.76	0.00	3.18	2.32
1,8-cineole	40.99	11.95	6.89	18.19	20.20
α-terpineol	17.49	15.19	5.81	14.66	12.72
Total specific activity [pkat/mg]	75.06	40.73	14.65	50.31	46.24
α-terpineol/1,8-cineole ratio	1 : 2.4	1 : 0.8	1 : 1.2	1 : 1.2	1 : 1.6

C ***Nicotiana langsdorffii***

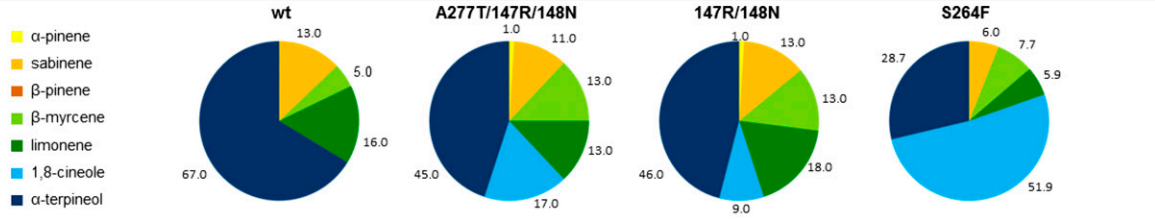

Specific activity [pkat/mg]				
α-pinene	0.00	0.71	0.28	0.00
sabinene	0.36	9.28	5.50	1.67
β-pinene	0.00	0.00	0.00	0.00
β-myrcene	0.14	10.68	5.36	2.13
limonene	0.46	10.50	7.40	1.64
1,8-cineole	0.00	11.48	3.93	12.59
α-terpineol	1.92	33.33	19.26	7.01
Total specific activity [pkat/mg]	2.87	75.99	71.74	25.02
α-terpineol/1,8-cineole ratio	1 : 0	1 : 0.4	1 : 0.2	1 : 1.8

Figure 3. Volatile profiles and specific enzyme activities of wild-type and mutant enzymes of *N. forgetiana*, *N. suaveolens*, and *N. langsdorffii*. Enzymes of *N. forgetiana* (A), *N. suaveolens* (B), and *N. langsdorffii* (C) were overexpressed in *E. coli* and purified via affinity chromatography (Supplemental Figs. S3 and S4); crude extracts were used for the *N. langsdorffii* wild type, 147R/148N, and S264F. The pie charts present the distribution (%) of each monoterpene released by wild-type and mutant enzymes. Specific enzyme activities (pkat mg^{-1}) were calculated for each monoterpene and summed up to total specific activities. The α-terpineol-to-1,8-cineole ratio is presented at the bottom in each part.

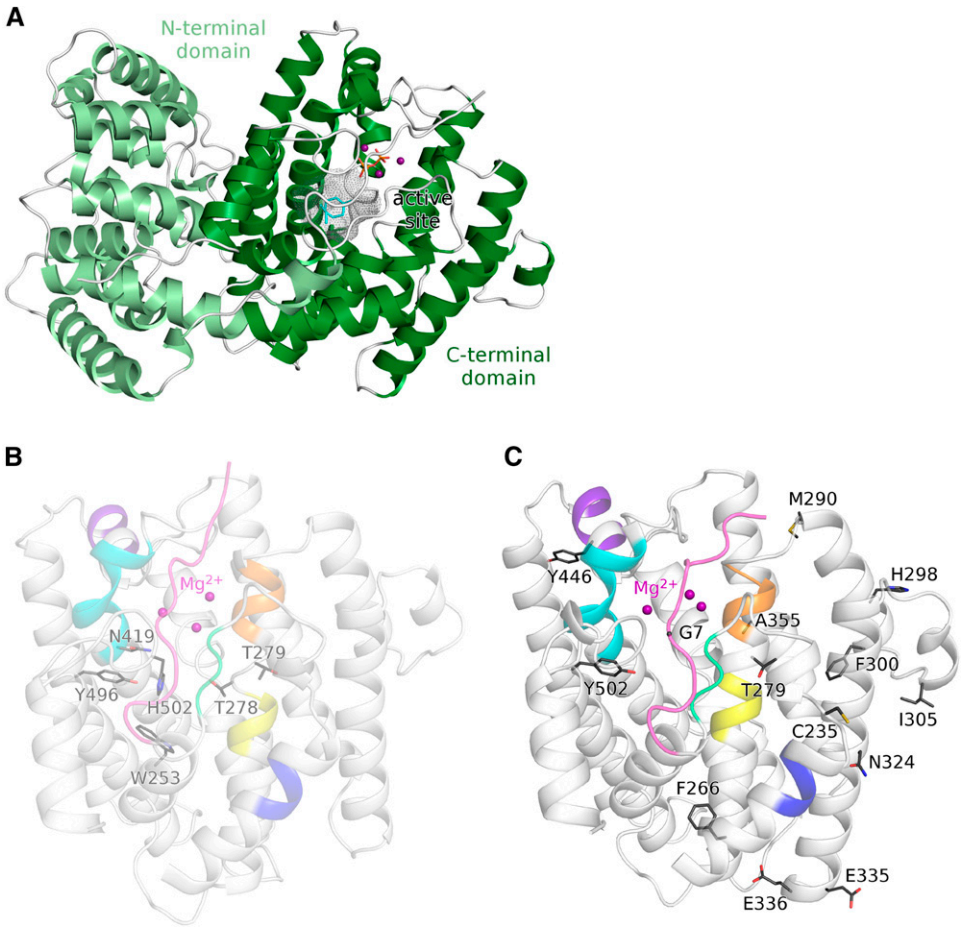

Figure 4. Homology models of 1,8-cineol synthases of *N. forgetiana* and *N. suaveolens*. A, The helices of the C- and N-terminal domains of the *N. forgetiana* cineol synthase are shown in green and light green, respectively. The α-terpinyl cation (cyan) and the diphosphate (orange) are presented as sticks. Violet dots represent the three magnesium ions (magnesium cluster). The mesh shows the surface of the cavity, which contains the putative active site. B, C-terminal domain of the *N. forgetiana* 3D model. Stick representation is used for mutated amino acids. The trinuclear magnesium cluster (violet) marks the active site. Colored cartoon regions represent conserved motifs: RR(X)$_8$W motif, pink; RWW motif, blue; RDR motif, green; NALV motif, yellow; DDxxD motif, orange; NSE/DTE motif, cyan; CYMNE motif, purple. Mutated amino acids and motifs shown correspond to Figure 2. Also shown is the N terminus covering the active site (pink line). C, C-terminal domain of the *N. suaveolens* 3D model with mutated amino acids and motifs. Coloring is as in B.

profile was identical to the in planta emission spectrum (Fähnrich et al., 2012). Additionally, geraniol, linalool, and in low amounts β-ocimene were detected in the in vitro assay. These acyclic monoterpene alcohols do not belong to the cineole cassette and may occur spontaneously by hydrolysis of the substrate GPP, as shown in negative controls. Therefore, these compounds were not considered further.

A homology model (Supplemental Fig. S5; Supplemental Table S11) of the *N. forgetiana* CIN was created, and the last known common intermediate in the synthesis of terpineol and cineole, the α-terpinyl cation, was placed in the active site (Fig. 4, A and B). Since the stereospecificity of this intermediate is still unknown, both enantiomers were treated equally during the following considerations. The back of the α-terpinyl cation is located on a hydrophobic patch at the bottom of the active site, while the tertiary cation in C7 of the α-terpinyl cation is stabilized by cation-π stacking upon the indole ring of Trp-253 (Fig. 5). In vitro tests of the mutant W253A revealed a strongly decreased amount of cyclic monoterpenes (Supplemental Tables S8–S10). Therefore, we conclude cation-π stacking to be crucial for the stabilization of the α-terpinyl cation and, thus, for the formation of all cyclic monoterpenes of the cineole cassette. An exchange to Met (W253M) did not seem to provide a comparable stabilization (Supplemental Tables S8–S10).

By in silico modeling, a water molecule was identified that is able to attack the α-terpinyl cation at its C7. Within the active site of the protein, the water is fixed by hydrogen bonds to the amino acid side chains of His-502 and Thr-278 (Fig. 6). During geometry optimization of the active site of this protein, using the semiempirical method PM7 (Stewart, 2013), the water nucleophilicity attacks the α-terpinyl cation without any energy barrier (Supplemental Fig. S5). During this attack, a putative catalytic dyad comprising His-502 and Glu-249 could

Table I. *Biochemical characterization of the wild-type and three mutant enzymes, F266S, F266T, and F266V, of N. suaveolens*

The enzyme assay using [^{3}H]GPP was performed with 1 μg of purified enzyme in a total volume of 50 μL. The results for V_{max} (μM min^{-1}), E_0 (M), k_{cat} (s^{-1}), K_m (μM), and k_{cat}/K_m (s^{-1} M^{-1}) were taken from Lineweaver-Burk plots. For the wild type, $n = 1$; for mutants F266S, F266T, and F266V, $n = 3$.

Enzyme	K_m	V_{max}	E_0	k_{cat}	k_{cat}/K_m
Wild type	0.19	0.008	3.4×10^{-7}	4.1×10^{-4}	2,157
F266S	0.12	0.006		2.9×10^{-4}	2,416
F266T	0.04	0.0012		5.8×10^{-5}	1,450
F266V	0.04	0.0017		8×10^{-5}	2,000

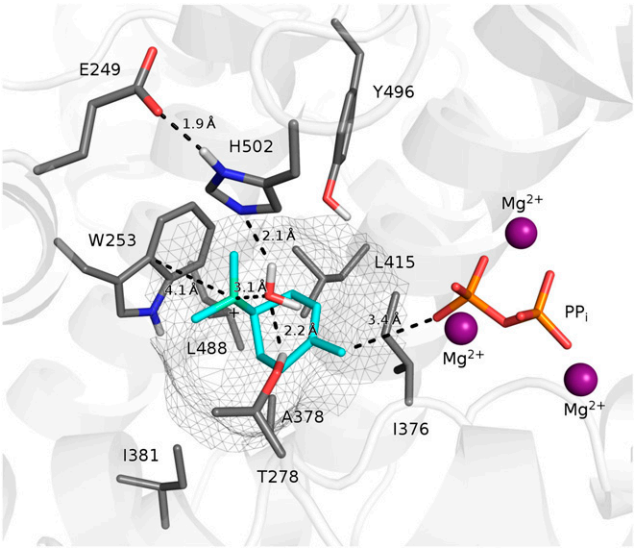

Figure 5. Active site of the cineole synthase of *N. forgetiana*. Amino acid side chains are shown as gray sticks. The back of the reactive intermediate α-terpinyl cation (cyan) is located on a hydrophobic patch (gray mesh), while the tertiary carbocation in C7 (green-cyan) exhibits a cation-π stack upon the indole ring of Trp-253. The C3 atom, where the prenyl moiety has been cleaved off in the last ionization step, is still in spatial proximity to the diphosphate (red-orange). A water molecule (red-white) is fixed by His-502 and Thr-278 and ready to perform a nucleophilic attack on the cationic C7 of the α-terpinyl cation.

act as a base, accepting one of the protons of the attacking water molecule. Interestingly, the mutation of this His (H502A) did not only lead to a decreased amount of cyclic products but also suppressed the formation of 1,8-cineole, thus producing α-terpineol as the main product (Supplemental Table S8). Monoterpenes that require as a last step in biosynthesis the abstraction of a proton need a specific proton acceptor in the active site as well (Fig. 1). The mechanism of the following cyclization of α-terpineol to 1,8-cineole depends strongly on the stereochemistry of the intermediate α-terpinyl cation. For both stereoisomers, semiempirical grid calculations suggest an autoprotonation of the α-terpineol and a subsequent ring closure to 1,8-cineole (Supplemental Fig. S6). The *R* isomer transfers its proton to the hydroxyl group of Tyr-496, which simultaneously protonates the double bond of the α-terpineol (Fig. 6). Using the *S* isomer as a starting point, the same proton relay occurs via the hydroxyl group of Thr-278 (Fig. 6). In our calculations, the energy barriers for these reaction paths are rather high (*R* isomer = 19.8 kcal mol^{-1} and *S* isomer = 19.7 kcal mol^{-1}; Supplemental Figs. S6 and S7).

The mutation of Tyr (Y496F) caused a drastic decrease of cyclic products (Fig. 3; Supplemental Tables S8–S10), suggesting a major role of this Tyr at an earlier step in the biosynthetic pathway. In addition, the hydroxyl group of this Tyr might be necessary to control the orientation of Asn-419. This Asn itself is proposed to be involved in binding and fixation of the diphosphate moiety of the substrate. The mutation N419A resulted in a drastic drop of enzyme activity, and except for traces of α-terpineol, no cyclic products were detected (Supplemental Tables S8–S10).

The product composition of the Thr mutant (T278A) was far more characteristic. In comparison with the wild-type enzyme, the most striking change was the decreased amount of 1,8-cineole (Supplemental Table S8). Thus, this mutation converted the wild-type cineole synthase into an α-terpineol synthase (Supplemental Table S10). Assuming that α-terpineol is a distinct precursor in the biosynthesis of 1,8-cineole, a decrease of cineole within the product profile indicated a disturbed reaction mechanism of the cyclization of α-terpineol toward 1,8-cineole. Therefore, we hypothesize a major role of Thr-278 in the formation of cineole by fixing the intermediate α-terpineol and supporting the

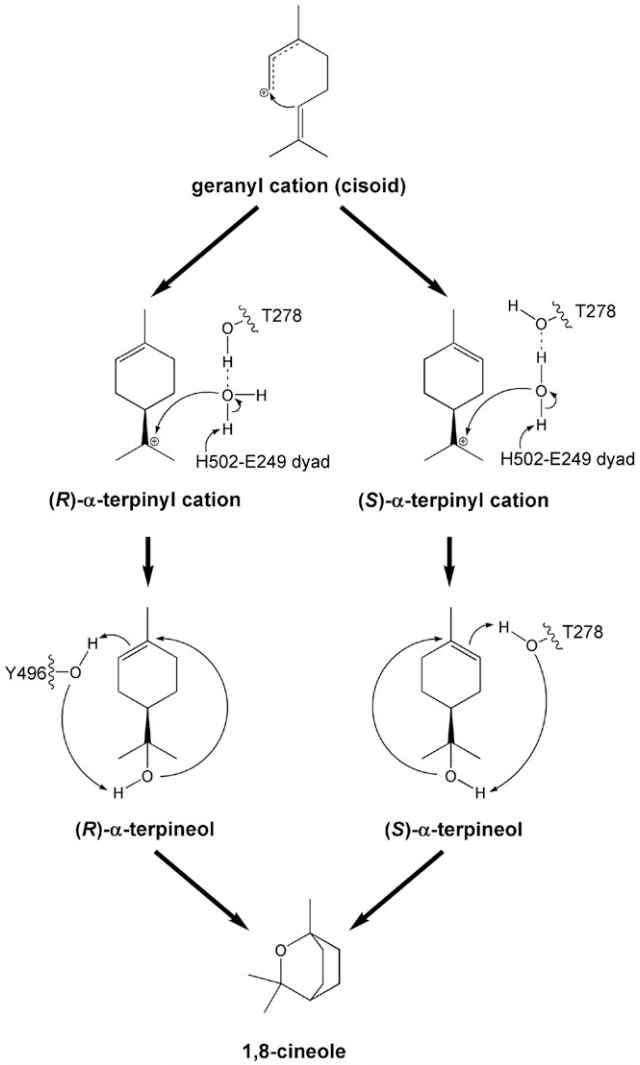

Figure 6. Proposed mechanism for the formation of 1,8-cineole. Depending on the stereochemistry of the intermediate, the protonation of the double bond of the α-terpinyl cation is provided by a proton relay via the hydroxyl groups of either Tyr-496 or Thr-278.

autoprotonation of its double bond. One sequence difference between *N. forgetiana* CIN and *N. langsdorffii* TER, in positions 279 and 277, respectively, is closest to the obviously important Thr-278, which is conserved in all CINs and TERs (Fig. 2). The mutation of this residue (T279A) did not change the product composition but led to an overall increase of activity in the *N. forgetiana* CIN (Supplemental Table S9).

Besides these theoretical considerations regarding reaction mechanism and pathways, we analyzed the enantiomers of α-terpineol produced by recombinant wild-type enzymes of five *Nicotiana* spp. (Table II). All five enzymes synthesized both enantiomers; however, the *S*-enantiomer was always dominant. Interestingly, the ratios appear conserved in the different species: for the CIN enzymes of *N. bonariensis*, *N. forgetiana*, and *N. suaveolens*, the *S*:*R* ratios were 6 to 8; for the TER of *N. alata*, it was 3; and in *N. langsdorffii* TER, it was 11. These results indicate that the route with the *S*-enantiomer is the preferred one.

DISCUSSION

Phe-266 Is Relevant for the Product Outcome of the 1,8-Cineole Synthase

It was demonstrated previously that single amino acid alterations of terpene synthases resulted in considerable product profile alterations. Kampranis et al. (2007) altered the 1,8-cineole synthase of *Salvia officinalis* into an α-terpineol synthase and sesquiterpene synthase. Garms et al. (2012) and Zhuang et al. (2012) demonstrated that a single amino acid substitution near the active pocket altered the product outcome for the sesquiterpene synthases SbTPS1 and SbTPS2 of *Sorghum bicolor*. Here, we showed that a single amino acid mutation (F266S), changing the large aromatic side chain of Phe into the small, hydroxylated amino acid Ser, resulted in a significant reduction of the second cyclization reaction in the CIN of *N. suaveolens* (Fig. 3). The reverse mutation from Ser to Phe of the TER of *N. langsdorffii* changed the profile toward 1,8-cineole as the major compound. Furthermore, insertion of Arg-147 and Asn-148, and both insertions in combination with the mutation A277T, also increased 1,8-cineole levels compared with the wild-type TER.

It is unclear how amino acid 266 and insertions at positions 147/148 influence the catalytic mechanism. A direct alteration of the active cavity seems unlikely, due to the large distance between these amino acids and the active site of greater than 10 Å and greater than 20 Å, respectively. However, second-tier amino acids can affect the active site geometry and catalysis of enzymes (Hyatt and Croteau, 2005; Greenhagen et al., 2006), as reported for the oxidosqualene cyclase, where the catalytic distinction between cycloartenol and lanosterol synthase activity was critical (Lodeiro et al., 2004). In the case of position 266 in *N. suaveolens*, the changed product specificity might be the result of either a change in the relative spatial orientation of the neighboring helices or a change in the hydrogen bond network. Position 266 is located in an α-helix, which also forms the active site and contains important amino acids such as Thr-278 and the DDXXD motif. That is why a change of the spatial orientation of this helix might affect the active site as well.

Further mutational analyses at position 266 were performed to determine which of the properties or structures of amino acids are responsible for the change in the product profile. Interestingly, 1,8-cineole remained the major product in the F266Y and F266T mutants with aromatic and/or hydroxylated amino acid substitutions (Fig. 3; Supplemental Tables S5–S7), supporting the hypothesis that the size differences of the amino acid side chain of F266S result in a loose coordination of α-terpineol, which could be released subsequently before being converted into 1,8-cineole. However, not in line with this interpretation is the observation that the small amino acid Val at this position did not favor α-terpineol release. At this point, we can only speculate that additional, yet unknown features besides size and H-bond network influence the reactions in the active pocket. Crystal structure analysis might shed light on this issue. Contradictory results also were obtained when *N. suaveolens* F266C and other monoterpene synthases with Cys at this position were compared. The α-terpineol synthases from *Magnolia grandiflora* (Lee and Chappell, 2008) or *Vitis vinifera* (Martin and Bohlmann, 2004) favor α-terpineol synthesis, while the mutant enzyme F266C of *N. suaveolens*, like the wild-type enzyme, produced more 1,8-cineole (data not shown). Also, the *Citrus unshiu* 1,8-cineole synthase carries a Cys at the corresponding position (Shimada et al., 2005). At the present state of knowledge, we conclude that Cys at this position in the helix has similar structural and functional properties to Phe.

With the help of domain-swapping experiments, it has been possible to show that the N-terminal domain does not determine the product spectra of monoterpene synthases (Peters and Croteau, 2003). Therefore, it is hard to evaluate potential structural changes caused by the insertion of Arg-147 and Asn-148 in *N. langsdorffii*.

Table II. *Amounts and ratios of α-terpineol enantiomers*

Recombinant enzymes were overexpressed in *E. coli*. Crude extracts were incubated with the substrate GPP, and products were analyzed by gas chromatography-mass spectrometry (GC-MS) using a stereoselective column (see "Materials and Methods"). Enantiomers were identified using commercially available compounds. Concentrations were determined according to an internal standard. $n = 2$.

Species	(*S*)-(−)-α-Terpineol	(*R*)-(+)-α-Terpineol	*S*:*R* Ratio
	$ng\ \mu L^{-1}$		
N. langsdorffii TER	0.330	0.029	11.2:1
	0.588	0.054	10.8:1
N. alata TER	0.081	0.025	3.2:1
	0.049	0.017	2.8:1
N. bonariensis CIN	0.488	0.067	7.3:1
	1.121	0.176	6.4:1
N. forgetiana CIN	1.175	0.149	7.9:1
	2.964	0.387	7.7:1
N. suaveolens CIN	1.266	0.191	6.6:1
	2.244	0.346	6.5:1

Proposed Catalytic Mechanism

Homology modeling and semiempiric calculations enabled us to suggest an enzymatic reaction mechanism for the formation of α-terpineol and 1,8-cineole in *N. forgetiana* CIN. After ionization and intramolecular addition of the linalyl diphosphate, the resulting α-terpinyl cation is stabilized by cation-π interactions with Trp-253. A water molecule, which forms hydrogen bonds between the side chain of Thr-278 and His-502, was detected in the active site based on the homology modeling, which also includes explicit water molecules. This water molecule is activated by proton abstraction supported by the catalytic dyad His-502 and Glu-249. During the nucleophilic attack of a water molecule on the α-terpinyl cation, one proton is transferred to a putative catalytic dyad comprising His-502 and Glu-249, resulting in α-terpineol. Finally, a hydroxyl group of an amino acid side chain (Tyr-496 or Thr-278) within the active site provides a proton relay to facilitate the autoprotonation of the double bond of α-terpineol. The following ring closure yields 1,8-cineole (Fig. 1).

A Trp, which is able to stabilize the intermediate cation, can be found in all monoterpene synthases of known structure at a position corresponding to Trp-253 in *N. forgetiana*. Mutation of this Trp decreased the amount of limonene and increased the amount of acyclic compounds in the product composition of the (4*S*)-limonene synthase (Srividya et al., 2015). Those authors also discussed a potential role of the Trp as an interaction partner of the intermediate cation. In the same enzyme, a His residue, corresponding to His-502 of *N. forgetiana*, was proposed either to provide stabilization of the cation or to act as a base, abstracting a proton at the final step of limonene biosynthesis (Srividya et al., 2015). Earlier experiments using His inhibitors already pointed toward the relevance of this amino acid in terpene synthases (Rajaonarivony et al., 1992). However, despite the need of a proton acceptor in most monoterpene synthases, this amino acid is not conserved throughout the monoterpene synthase family.

Our proposed mechanism is in accordance with the experimental results of Wise et al. (2002), which revealed a *syn* addition to the double bond in the 1,8-cineole synthase of *S. officinalis*. In our theory, the autoprotonation of the double bond does not happen directly, as proposed by Wise et al. (2002), but via a proton relay. They also suggested that the deprotonation of the hydroxyl group takes place after the final ring closure to 1,8-cineole. Although this idea is very intriguing because of the higher acidity of the α-terpinyl hydronium ion, in all our simulations, the proton is abstracted during the nucleophilic attack of the water.

(*R*)-(+)- or (*S*)-(−)-(α)Terpinyl Cation Intermediate

There are characterized monoterpene synthases specifically synthesizing the *R* or *S* intermediate: the CIN of *S. officinalis* also produces (*R*)-α-terpineol (Wise et al., 1998), whereas the Arabidopsis (*Arabidopsis thaliana*) CIN and the *V. vinifera* TER produce (*S*)-α-terpineol, suggesting the (*R*)- and (*S*)-α-terpinyl cation being the intermediate, respectively (Chen et al., 2004; Martin and Bohlmann, 2004). However, the stereochemistry of the intermediate α-terpinyl cation of other characterized cineole synthases (e.g. *C. unshiu* and *Lavandula* spp.) is still unknown (Shimada et al., 2005; Demissie et al., 2012). Even though the open-chain cationic intermediates are achiral, Croteau et al. (1994) pointed out that the stereochemical fate of the intermediate is already fixed upon binding and isomerization of the substrate GPP. Recently, in vitro experiments in self-assembled cavities clearly support that a direct isomerization of a geranyl cation to the cisoid-isomer is possible (Zhang and Tiefenbacher, 2015).

As we could determine the *S*-enantiomer of α-terpineol as the dominant compound released from the cineole and terpineol synthases of five *Nicotiana* spp. (Table II), this convincingly supported and clarified the actual stereochemistry of this reaction mechanism. Furthermore, the hypothesis of an (*S*)-α-terpinyl cation being attacked by a water molecule, resulting in (*S*)-α-terpineol, which protonates itself by a proton relay via Thr-278 and cyclizes to 1,8-cineole (Fig. 6), also was deduced from the mutant T278A, which specifically diminished the production of 1,8-cineole and subsequently demonstrated the special role of this amino acid in the second cyclization reaction (Figs. 3 and 5).

MATERIALS AND METHODS

Site-Directed Mutagenesis

For mutation experiments, *Nicotiana forgetiana* CIN and *Nicotiana suaveolens* CIN (Roeder et al., 2007; Fähnrich et al., 2012) were cloned into the pET SUMO expression vector (Invitrogen). Nucleotide changes were generated using the Quick Change Site Directed Mutagenesis Kit (Agilent) according to the manufacturer's recommendation. PCR parameters for *N. forgetiana* CIN were as follows: a 2-min initial denaturation at 95°C was followed by 16 cycles of denaturation at 95°C for 30 s, annealing at 55°C for 60 s, and elongation at 68°C for 12 min. Reactions were finished by a final elongation of 68°C for 10 min. PCR parameters for *N. suaveolens* CIN were slightly different: a 2-min initial denaturation at 97°C was followed by 18 cycles of denaturation at 97°C for 50 s, annealing at 55°C for 50 s, elongation at 68°C for 12 min, and a final elongation of 10 min at 68°C. The primers used are shown in Supplemental Table S13. PCR was followed by adding 1 μL of *Dpn*I (10 units μL^{-1}) restriction enzyme to the reaction tubes for the digestion of methylated and unmutated parental DNA templates. The digestion was carried out for 90 min at 37°C. One microliter of mutated plasmids was used for the transformation into *Escherichia coli* TOP10 cells (Invitrogen). Plasmids were reisolated from single *E. coli* TOP10 clones using the NucleoSpin Plasmid Easy Pure Kit (Macherey-Nagel), and mutated sequences were confirmed by Sanger sequencing (GATC Biotech).

Heterologous Protein Expression

The proteins were expressed using the Champion pET SUMO Protein Expression System (Invitrogen). Expression and purification were carried out as described by Hippauf et al. (2010). *E. coli* HMS 174 (DE3) strain (Novagen) was used for the overexpression of His_6-tagged proteins. Overexpressed protein was obtained after a preincubation of 150 mL of culture at 37°C until OD_{600} of 0.6 and 1 was reached for *N. forgetiana* and *N. suaveolens*, respectively. *E. coli* HMS 174 (DE3) cells were induced with 0.5 mM isopropylthio-β-galactoside, and the incubation was continued for 20 h at 20°C. Crude extracts were obtained by incubating the cell pellet with lysozyme (final concentration, 1 mg mL^{-1}), sonication, and centrifugation in order to separate cell debris from the enzyme containing soluble fraction. The overexpressed protein was purified by Ni-NTA affinity chromatography (Qiagen) according to the manufacturer's instructions. Protein concentrations were measured using the

standard Bradford assay. Protein purification was checked using SDS-PAGE and western blotting (anti-His tag antibody and anti-rabbit IgG; Sigma)

Enzyme Assay

For enzyme tests using *N. forgetiana* CIN wild-type and mutated enzymes, 60 μg of purified enzyme, 60 μL of assay buffer (250 mM HEPES-KOH buffer [pH 8], 100 mM $MgCl_2$, 2.5 mM $MnCl_2$, and 50% glycerol), 5 μL of DTT (1 M) and 40 μL of 1 μg μL^{-1} GPP (Echelon Biosciences) were supplemented with water to a final volume of 250 μL and incubated at 39°C for 3 h. The assay samples were overlaid with 250 μL of hexane containing 5 ng μL^{-1} cis-nerolidol (Carl Roth) as an internal standard. The products were extracted by vortexing for 30 s followed by centrifugation (5 min at 4,000*g*). One microliter of the hexane phase was used for GC-MS analysis.

For enzyme tests using *N. suaveolens* CIN wild-type and mutated enzymes, 10 μg of *E. coli* crude extract and purified enzyme, respectively, 40 μL assay buffer (250 mM HEPES-KOH buffer [pH 8], 100 mM $MgCl_2$, 2.5 mM $MnCl_2$, and 50% glycerol), 5 μL of 1 M DTT, and 4 μL of 1 μg μL^{-1} GPP (Echelon Biosciences) were mixed with water to a final volume of 200 μL and incubated at 41.5°C for 3 h. The assay samples were overlaid with 200 μL of hexane supplemented with 5 ng μL^{-1} cis-nerolidol (Carl Roth) as an internal standard. The products were extracted by vortexing for 30 s and centrifugation (1 min at 4,000*g*). One microliter of the hexane phase was used for GC-MS analysis.

The biochemical parameters V_{max}, K_m, and k_{cat} were determined using different substrate concentrations (10, 20, 30, 40, 50, and 60 nM). The product formation was monitored between 2 and 10 min. The initial rate (i.e. the linear range) of each substrate concentration was plotted in a Lineweaver-Burk diagram. The assay was performed in a total volume of 50 μL with 10 μL of 5× HEPES buffer, 1 μL of substrate [^{3}H]GPP (1 mCi mL^{-1}; Hartmann Analytics), 1 μg of enzyme, and 2.5 mM DTT, overlaid with 180 mL of hexane, and incubated at 41.5°C. The reaction was stopped by transferring it on ice for 15 s, mixing (1 min), and centrifugation (2 min at 13,000 rpm). Fifty microliters of the organic phase was added to 2 mL of scintillation solution (Ultima Gold; Perkin Elmer), and product formation was counted in Tricarb 2810TR (Perkin Elmer).

GC-MS Analysis

The volatile compounds were analyzed with a Shimadzu QP5000 gas chromatograph connected to a Shimadzu mass spectrometer for identification. Separation was performed on a DB-5MS column (60 m × 0.25 mm × 0.25 μm; Agilent) with helium as carrier gas (flow rate of 1.1 mL min^{-1}) using an injection temperature of 200°C and a temperature gradient from 35°C (2-min hold) to 280°C (15-min hold) with a ramp of 10°C min^{-1}. Mass spectra were obtained using the scan mode (total ion count, 40–280 mz^{-1}). Compound identity was confirmed by comparison of the obtained spectra with spectra in the library of the National Institute of Standards and Technology (NIST147) and with spectra obtained from authentic standards. Enantiomers of α-terpineol were separated employing the 7890A gas chromatograph coupled to a 5975C mass selective detector (Agilent), which was equipped with an enantioselective column coated with heptakis(6-*O*-*tert*-butyldimethylsilyl-2,3-di-*O*-methyl)-β-cyclodextrin (50% [w/w] in OV17, 25 m × 0.25 mm i.d.; König et al., 1994). The sample was injected in split mode with a split flow of 20 mL min^{-1}, an injection temperature of 250°C, and a column flow of 1.2 mL min^{-1}. The separation started with an initial temperature of 50°C for 1 min followed by a ramp of 2°C min^{-1} to a final temperature of 170°C. The mass range was set from 45 to 300 mz^{-1} with a scan speed of 5.4 scans s^{-1}. Identity was confirmed by comparing the mass spectra with the National Institute of Standards and Technology library and with those of authentic standards.

Homology Modeling

Sequences of *N. forgetiana* CIN, *N. suaveolens* CIN, and *Nicotiana langsdorffii* TER were published recently (Roeder et al., 2007; Fähnrich et al., 2011, 2012) and correspond to UniProt codes I7CTV3, A5Y5L5, and H2ELN1, respectively. The sequences have been truncated to the mature protein, starting with the $RR(x)_8W$ motif. For homology model creation, automated modeling by Yasara (Krieger et al., 2009) was used with default settings. Due to errors in the interpretation of ligand double bonds, the templates were not taken from pdb redo (default) but downloaded from rcsb pdb and provided manually. For further work, the hybrid models, containing features derived from all given templates, were used. All homology models were energy optimized using the force field Yasara2 (Krieger at al., 2002) as implemented in Yasara. The model of *N. forgetiana* CIN was refined by a molecular dynamics simulation (MD) for 7.5 ns using the force field Amber03 (Duan et al., 2003). Due to problems regarding the backbone dihedrals in loop N160-A168, this loop was taken over from the model of *N. langsdorffii* TER into the mean structure of the production phase of the MD. To minimize deviations from planarity of the peptide bonds, in a second MD (175 ns; Amber03), the force constant of the peptide dihedral was increased by a factor of 1.5. After each modeling step, the models were evaluated by the model quality assessment programs Prosa (Sippl, 1990), Procheck (Laskowski et al., 1993), and QMEAN (Benkert et al., 2008).

Due to missing parameters for the carbocation in established docking programs, the reactive intermediates (*R*)- and (*S*)-α-terpinyl cation were positioned in the putative active site manually. Since the automated parameterization of Yasara failed for the intermediates, these intermediates were parameterized with AM1-BCC (Jakalian et al., 2002) and Gaff (Wang et al., 2004) using Antechamber and SQM (Case et al., 2012). The models were put into water boxes, and while fixing all heavy atoms of the receptor and ligand, the system was relaxed with an MD (2 ns; Amber03).

For the semiempirical calculations, the model was reduced to active site residues and ligands. The elucidation of the reaction mechanism was performed with the help of grid calculations using PM7 (Stewart, 2013) as implemented in MOPAC (Stewart, 1990). For both stereoisomers of the intermediate, different combinations of reaction coordinates were examined.

Accession Numbers

Sequence data from this article can be found in the GenBank/EMBL data libraries under the following accession numbers: *N. suaveolens*, EF175166.1; *N. forgetiana*, JX028206.1; *N. bonariensis*, JX028207.1; *N. longiflora*, JX040448.1; *N. mutabilis*, JX040449.1; *N. alata*, JQ346173.1; and *N. langsdorffii*, JN989317.1.

Supplemental Data

The following supplemental materials are available.

Supplemental Figure S1. Analysis of volatile profiles, enzyme activities, and terpineol-cineole ratios in the mutants and wild-type cineole synthase (*E. coli* crude extract) of *N. suaveolens*.

Supplemental Figure S2. SDS-PAGE and western blot of the purified wild-type and mutant (F266S, F266T, and F266V) enzymes of *N. suaveolens*.

Supplemental Figure S3. Analysis of volatile profiles, enzyme activities, and terpineol-cineole ratio of mutants of terpineol synthase (*E. coli* crude extract) of *N. langsdorffii*.

Supplemental Figure S4. Purification of the recombinant wild-type and mutant cineole synthase of *N. forgetiana*.

Supplemental Figure S5. Supporting calculations for the 3D model of cineole synthase of *N. forgetiana*.

Supplemental Figure S6. MOPAC grid calculations to examine the energy barriers of the reaction path from α-terpineol to 1,8-cineole of *N. forgetiana*.

Supplemental Figure S7. Reaction path from α-terpinyl cation to 1,8 cineole in *N. forgetiana*.

Supplemental Table S1. Terpineol and cineole synthase amino acid sequence identities and number of different amino acids of various *Nicotiana* spp.

Supplemental Table S2. Amino acid alterations in terpineol and cineole synthases of *Nicotiana* spp.

Supplemental Table S3. Mutants constructed of cineole synthase of *N. suaveolens*.

Supplemental Table S4. Distribution of monoterpene products, specific enzyme activities, and α-terpineol-to-1,8-cineole ratios of wild-type and mutated enzymes of *N. suaveolens*.

Supplemental Table S5. Amounts of products synthesized by the wild-type and mutated enzymes of *N. suaveolens*.

Supplemental Table S6. Specific enzyme activities of the wild-type and mutated enzymes of *N. suaveolens*.

Supplemental Table S7. Relative enzyme activities of *N. suaveolens* wild-type and mutant enzymes.

Supplemental Table S8. Amounts of product synthesized by the wild-type and mutated enzymes of *N. forgetiana*.

Supplemental Table S9. Specific enzyme activities of the wild-type and mutated enzymes of *N. forgetiana*.

Supplemental Table S10. Relative enzyme activities of *N. forgetiana* wild-type and mutant enzymes.

Supplemental Table S11. Templates used for homology modeling.

Supplemental Table S12. Biochemical parameters of cineole synthases of different plant species and a limonene synthase of *Mentha spicata*.

Supplemental Table S13. Primer sequences to generate *N. forgetiana* and *N. suaveolens* mutants.

ACKNOWLEDGMENTS

We thank Claudia Dinse (University of Rostock) for technical assistance; Francel Verstappen (University of Wageningen) for enantiomer separation; Marco Kai and Sybille Lorenz for analyzing wild-type enzymes with terpineol as substrate; Aleš Svatoš for allowing us to use his GC-MS device for the latter measurements; and master students Madeleine Neumann and Madlen Klodt, who performed the experiments with *N. langsdorffii*.

Received September 8, 2016; accepted October 5, 2016; published October 11, 2016.

LITERATURE CITED

Benkert P, Tosatto SC, Schomburg D (2008) QMEAN: a comprehensive scoring function for model quality assessment. Proteins **71:** 261–277

Bohlmann J, Keeling CI (2008) Terpenoid biomaterials. Plant J **54:** 656–669

Case DA, Darden TA, Cheatham TE III, Simmerling CL, Wang J, Duke RE, Luo R, Walker RC, Zhang W, Merz KM, et al (2012) AMBER 12. University of California, San Francisco

Chen F, Ro DK, Petri J, Gershenzon J, Bohlmann J, Pichersky E, Tholl D (2004) Characterization of a root-specific *Arabidopsis* terpene synthase responsible for the formation of the volatile monoterpene 1,8-cineole. Plant Physiol **135:** 1956–1966

Christianson DW (2006) Structural biology and chemistry of the terpenoid cyclases. Chem Rev **106:** 3412–3442

Croteau R, Alonso WR, Koepp AE, Johnson MA (1994) Biosynthesis of monoterpenes: partial purification, characterization, and mechanism of action of 1,8-cineole synthase. Arch Biochem Biophys **309:** 184–192

Degenhardt J, Köllner TG, Gershenzon J (2009) Monoterpene and sesquiterpene synthases and the origin of terpene skeletal diversity in plants. Phytochemistry **70:** 1621–1637

Demissie ZA, Cella MA, Sarker LS, Thompson TJ, Rheault MR, Mahmoud SS (2012) Cloning, functional characterization and genomic organization of 1,8-cineole synthases from *Lavandula*. Plant Mol Biol **79:** 393–411

Duan Y, Wu C, Chowdhury S, Lee MC, Xiong G, Zhang W, Yang R, Cieplak P, Luo R, Lee T, et al (2003) A point-charge force field for molecular mechanics simulations of proteins based on condensed-phase quantum mechanical calculations. J Comput Chem **24:** 1999–2012

Fähnrich A, Brosemann A, Teske L, Neumann M, Piechulla B (2012) Synthesis of 'cineole cassette' monoterpenes in *Nicotiana* section *Alatae*: gene isolation, expression, functional characterization and phylogenetic analysis. Plant Mol Biol **79:** 537–553

Fähnrich A, Krause K, Piechulla B (2011) Product variability of the 'cineole cassette' monoterpene synthases of related Nicotiana species. Mol Plant **4:** 965–984

Fähnrich A, Neumann M, Piechulla B (2014) Characteristic alatoid 'cineole cassette' monoterpene synthase present in *Nicotiana noctiflora*. Plant Mol Biol **85:** 135–145

Garms S, Chen F, Boland W, Gershenzon J, Köllner TG (2012) A single amino acid determines the site of deprotonation in the active center of sesquiterpene synthases SbTPS1 and SbTPS2 from *Sorghum bicolor*. Phytochemistry **75:** 6–13

Gershenzon J, Dudareva N (2007) The function of terpene natural products in the natural world. Nat Chem Biol **3:** 408–414

Greenhagen BT, O'Maille PEO, Noel JP, Chappell J (2006) Identifying and manipulating structural determinates linking catalytic specificities in terpene synthases. Proc Natl Acad Sci USA **103:** 9826–9831

Hippauf F, Michalsky E, Huang R, Preissner R, Barkman TJ, Piechulla B (2010) Enzymatic, expression and structural divergences among carboxyl O-methyltransferases after gene duplication and speciation in *Nicotiana*. Plant Mol Biol **72:** 311–330

Hyatt DC, Croteau R (2005) Mutational analysis of a monoterpene synthase reaction: altered catalysis through directed mutagenesis of (−)-pinene synthase from *Abies grandis*. Arch Biochem Biophys **439:** 222–233

Jakalian A, Jack DB, Bayly CI (2002) Fast, efficient generation of high-quality atomic charges. AM1-BCC model. II. Parameterization and validation. J Comput Chem **23:** 1623–1641

Kampranis SC, Ioannidis D, Purvis A, Mahrez W, Ninga E, Katerelos NA, Anssour S, Dunwell JM, Degenhardt J, Makris AM, et al (2007) Rational conversion of substrate and product specificity in a *Salvia* monoterpene synthase: structural insights into the evolution of terpene synthase function. Plant Cell **19:** 1994–2005

König WA, Rieck A, Hardt I, Gehrcke B, Kubeczka KH, Muhle H (1994) Enantiomeric composition of the chiral constituents of essential oils. Part 2. Sesquiterpene hydrocarbons. J High Resolut Chromatogr **17:** 315–320

Krieger E, Joo K, Lee J, Lee J, Raman S, Thompson J, Tyka M, Baker D, Karplus K (2009) Improving physical realism, stereochemistry, and side-chain accuracy in homology modeling: four approaches that performed well in CASP8. Proteins (Suppl 9) **77:** 114–122

Krieger E, Koraimann G, Vriend G (2002) Increasing the precision of comparative models with YASARA NOVA: a self-parameterizing force field. Proteins **47:** 393–402

Laskowski RA, Macarthur MW, Moss DS, Thornton JM (1993) Procheck: a program to check the stereochemical quality of protein structures. J Appl Cryst **26:** 283–291

Lee S, Chappell J (2008) Biochemical and genomic characterization of terpene synthases in *Magnolia grandiflora*. Plant Physiol **147:** 1017–1033

Lodeiro S, Segura MJR, Stahl M, Schulz-Gasch T, Matsuda SPT (2004) Oxidosqualene cyclase second-sphere residues profoundly influence the product profile. ChemBioChem **5:** 1581–1585

Martin DM, Bohlmann J (2004) Identification of *Vitis vinifera* (−)-alpha-terpineol synthase by *in silico* screening of full-length cDNA ESTs and functional characterization of recombinant terpene synthase. Phytochemistry **65:** 1223–1229

Peters RJ, Croteau RB (2003) Alternative termination chemistries utilized by monoterpene cyclases: chimeric analysis of bornyl diphosphate, 1,8-cineole, and sabinene synthases. Arch Biochem Biophys **417:** 203–211

Raguso RA, Schlumpberger BO, Kaczorowski RL, Holtsford TP (2006) Phylogenetic fragrance patterns in *Nicotiana* sections Alatae and Suaveolentes. Phytochemistry **67:** 1931–1942

Rajaonarivony JI, Gershenzon J, Miyazaki J, Croteau R (1992) Evidence for an essential histidine residue in 4*S*-limonene synthase and other terpene cyclases. Arch Biochem Biophys **299:** 77–82

Roeder S, Hartmann AM, Effmert U, Piechulla B (2007) Regulation of simultaneous synthesis of floral scent terpenoids by the 1,8-cineole synthase of *Nicotiana suaveolens*. Plant Mol Biol **65:** 107–124

Shimada T, Endo T, Fujii H, Hara M, Omura M (2005) Isolation and characterization of (*E*)-beta-ocimene and 1,8-cineole synthases in *Citrus unshiu* Marc. Plant Sci **168:** 987–995

Sippl MJ (1990) Calculation of conformational ensembles from potentials of mean force: an approach to the knowledge-based prediction of local structures in globular proteins. J Mol Biol **213:** 859–883

Srividya N, Davis EM, Croteau RB, Lange BM (2015) Functional analysis of (4*S*)-limonene synthase mutants reveals determinants of catalytic outcome in a model monoterpene synthase. Proc Natl Acad Sci USA **112:** 3332–3337

Starks CM, Back K, Chappell J, Noel JP (1997) Structural basis for cyclic terpene biosynthesis by tobacco 5-epi-aristolochene synthase. Science **277:** 1815–1820

Stewart JJP (1990) MOPAC: a semiempirical molecular orbital program. J Comput Aided Mol Des **4:** 1–105

Stewart JJP (2013) Optimization of parameters for semiempirical methods. VI. More modifications to the NDDO approximations and re-optimization of parameters. J Mol Model **19:** 1–32

Thompson JD, Higgins DG, Gibson TJ (1994) CLUSTAL W: improving the sensitivity of progressive multiple sequence alignment through sequence weighting, position-specific gap penalties and weight matrix choice. Nucleic Acids Res **22:** 4673–4680

Turner G, Gershenzon J, Nielson EE, Froehlich JE, Croteau R (1999) Limonene synthase, the enzyme responsible for monoterpene biosynthesis in

peppermint, is localized to leucoplasts of oil gland secretory cells. Plant Physiol **120:** 879–886

Wang J, Wolf RM, Caldwell JW, Kollman PA, Case DA (2004) Development and testing of a general amber force field. J Comput Chem **25:** 1157–1174

Williams DC, McGarvey DJ, Katahira EJ, Croteau R (1998) Truncation of limonene synthase preprotein provides a fully active 'pseudomature' form of this monoterpene cyclase and reveals the function of the amino-terminal arginine pair. Biochemistry **37:** 12213–12220

Wise ML, Savage TJ, Katahira E, Croteau R (1998) Monoterpene synthases from common sage (*Salvia officinalis*): cDNA isolation, characterization, and functional expression of (+)-sabinene synthase, 1,8-cineole synthase, and (+)-bornyl diphosphate synthase. J Biol Chem **273:** 14891–14899

Wise ML, Urbansky M, Helms GL, Coates RM, Croteau R (2002) *Syn* stereochemistry of cyclic ether formation in 1,8-cineole biosynthesis catalyzed by recombinant synthase from *Salvia officinalis*. J Am Chem Soc **124:** 8546–8547

Zhang Q, Tiefenbacher K (2015) Terpene cyclization catalysed inside a self-assembled cavity. Nat Chem **7:** 197–202

Zhuang X, Köllner TG, Zhao N, Li G, Jiang Y, Zhu L, Ma J, Degenhardt J, Chen F (2012) Dynamic evolution of herbivore-induced sesquiterpene biosynthesis in *Sorghum* and related grass crops. Plant J **69:** 70–80

Supporting information

The following materials are available in the online version of this article.

	mutant G7Q crude extract	mutant G7Q/M290L crude extract	mutant M290L crude extract	wild type crude extract
	specific activity [pkat/mg]			
sabinene	4.7	2 ± 0.2[b]	3.9 ± 1.7[a]	1.6 ± 1.5[a]
β-myrcene	2.7	2 ± 0.1[b]	5.8 ± 0.7[a]	2.1 ± 1.5[a]
limonene	2.3	1.4 ± 0[b]	3.6 ± 1[a]	1.6 ± 1.2[a]
1,8-cineole	20.2	11.7 ± 0.2[b]	29.1 ± 4.6[a]	15.4 ± 11[a]
α-terpineol	9.9	5.9 ± 0.7[b]	12.9 ± 1.7[a]	6.4 ± 4.1[a]
	total specific activity [pkat/mg]			
	39.9	23.2 ± 1[b]	55.3 ± 6.9[a]	27.2 ± 18.9[a]
	α-terpineol/1,8-cineole ratio			
	1 : 2.0	**1 : 2.0**	**1 : 2.3**	**1 : 2.4**
	distribution [%]			
	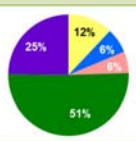	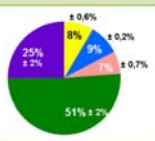	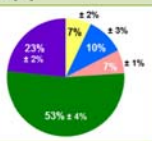	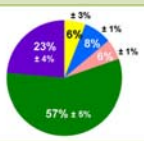

Supplemental **Figure S1A**: Analysis of volatile profiles (% distribution of monoterpenes), enzyme activities (pkat/mg) and terpineol/cineole ratios in the mutants G7Q, G7Q/M290L, M290L and wildtype cineole synthase (*E. coli* crude extract) of *Nicotiana suaveolens*

	mutant H298D 1 crude extract	mutant H298D 2 crude extract	mutant M290L/H298D 1 crude extract	mutant M290L/H298D 2 crude extract	wild type crude extract
	specific activity [pkat/mg]				
sabinene	0	2.3	0	0	1.6 ± 1.5[a]
β-myrcene	0	1.9	1.9	0	2.1 ± 1.5[a]
limonene	0	2.7	0.3	0	1.6 ± 1.2[a]
1,8-cineole	1.6	28	10.6	1.6	15.4 ± 11[a]
α-terpineol	0.4	11.3	5.3	1	6.4 ± 4.1[a]
	total specific activity [pkat/mg]				
	2	46.1	18.3	2.6	27.2 ± 18.9[a]
	α-terpineol/1,8-cineole ratio				
	1 : 4.0	**1 : 2.5**	**1 : 2.0**	**1 : 1.6**	**1 : 2.4**
	distribution [%]				
	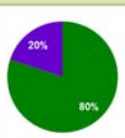	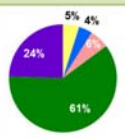	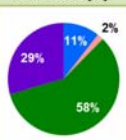	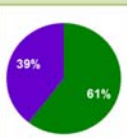	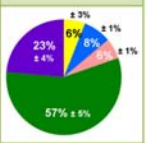

9

10 Supplemental **Figure S1B**: Analysis of volatile profiles (% distribution of monoterpenes),
11 enzyme activities (pkat/mg) and terpineol/cineole ratios in the mutants H298D and
12 M290L/H298D and wildtype cineole synthase (*E.coli* crude extract) of *Nicotiana suaveolens*

	mutant I305T 1 crude extract	mutant I305T 2 crude extract	mutant N324D 1 crude extract	mutant N324D 2 crude extract	wild type crude extract
	specific activity [pkat/mg]				
sabinene	2.1	0	0	4.3	1.6 ± 1.5[a]
β-myrcene	5.8	0	0.1	6.5	2.1 ± 1.5[a]
limonene	3.5	0	0.2	3.1	1.6 ± 1.2[a]
1,8-cineole	27.5	1.1	1.5	24.6	15.4 ± 11[a]
α-terpineol	11.7	0.3	0.6	11.4	6.4 ± 4.1[a]
	total specific activity [pkat/mg]				
	50.5	1.4	2.5	49.9	27.2 ± 18.9[a]
	α-terpineol/1,8-cineole ratio				
	1 : 2.3	**1 : 3.6**	**1 : 2.5**	**1 : 2.2**	**1 : 2.4**
	distribution [%]				
	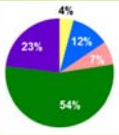	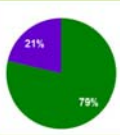	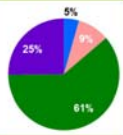	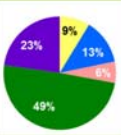	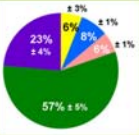

13

14 Supplemental **Figure S1C**: Analysis of volatile profiles (% distribution of monoterpenes),
15 enzyme activities (pkat/mg) and terpineol/cineole ratios in the mutants I305T and N324D and
16 wildtype cineole synthase (*E.coli* crude extract) of *Nicotiana suaveolens*

	mutant E335/336 deleted 1 crude extract	mutant EE335/336 deleted 2 crude extract	mutant A355S 1 crude extract	mutant A355S 2 crude extract	wild type crude extract
	specific activity [pkat/mg]				
sabinene	0.6	0	2.3	0	1.6 ± 1.5[a]
β-myrcene	0.9	0	2.8	0.1	2.1 ± 1.5[a]
limonene	0.6	0	2.1	0.05	1.6 ± 1.2[a]
1,8-cineole	4.3	6.3	21.6	3	15.4 ± 11[a]
α-terpineol	2	2.4	10	1	6.4 ± 4.1[a]
	total specific activity [pkat/mg]				
	8.4	8.7	38.9	4.1	27.2 ± 18.9[a]
	α-terpineol/1,8-cineole ratio				
	1 : 2.2	**1 : 2.6**	**1 : 2.2**	**1 : 3**	**1 : 2.4**
	distribution [%]				
	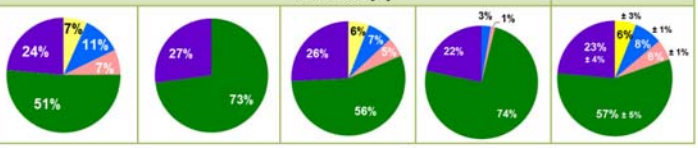				

17

18 Supplemental **Figure S1D**: Analysis of volatile profiles (% distribution of monoterpenes),
19 enzyme activities (pkat/mg) and terpineol/cineole ratios in the mutants E335/E336 and A355S
20 and wildtype cineole synthase (*E.coli* crude extract) of *Nicotiana suaveolens*

	mutant C235G crude extract	mutant T279A 1 crude extract	mutant T279A 2 crude extract	mutant Y446A crude extract	wild type crude extract
	specific activity [pkat/mg]				
sabinene	3.3	0	0	0	1.6 ± 1.5[a]
β-myrcene	5.4	0.5	0	0	2.1 ± 1.5[a]
limonene	4.3	0.2	0	0	1.6 ± 1.2[a]
1,8-cineole	28.4	4.2	3	0	15.4 ± 11[a]
α-terpineol	12	2.6	3.2	4.1	6.4 ± 4.1[a]
	total specific activity [pkat/mg]				
	53.4	7.5	10.6	18.5	27.2 ± 18.9[a]
	α-terpineol/1,8-cineole ratio				
	1 : 2.4	**1 : 1.6**	**1 : 1.6**	**1 : 1.6**	**1 : 2.4**
	distribution [%]				
	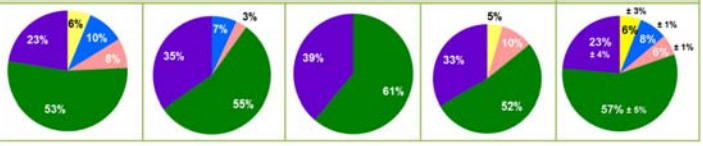				

21

22 Supplemental **Figure S1E**: Analysis of volatile profiles (% distribution of monoterpenes),
23 enzyme activities (pkat/mg) and terpineol/cineole ratios in the mutants C235G, T279A and
24 Y446A and wildtype cineole synthase (*E.coli* crude extract) of *Nicotiana suaveolens*

	mutant F266S crude extract 1 (n=2)	mutant F266S crude extract 2 (n=2)	mutant F266V crude extract 1	mutant F266V crude extract 2	wild type crude extract
	specific activity [pkat/mg]				
sabinene	1.1 ± 0.2[b]	0	0	0	1.6 ± 1.5[a]
β-myrcene	0.6 ± 0.1[b]	0	0	0	2.1 ± 1.5[a]
limonene	1 ± 0.4[b]	0	0	0	1.6 ± 1.2[a]
1,8-cineole	1.9 ± 0.1[b]	0	3	0	15.4 ± 11[a]
α-terpineol	4 ± 1[b]	2.4 ± 0.4[b]	3.2	4.1	6.4 ± 4.1[a]
	total specific activity [pkat/mg]				
	8.5 ± 1.5[b]	2.4 ± 0.4[b]	6.2	4.1	27.2 ± 18.9[a]
	α-terpineol/1,8-cineole ratio				
	1 : 0.5	**1 : 0**	**1 : 0.9**	**1 : 0**	**1 : 2.4**
	distribution [%]				
	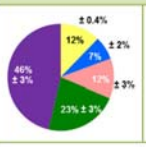		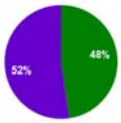		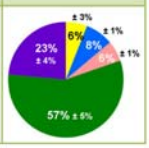

25

26 Supplemental **Figure S1F**: Analysis of volatile profiles (% distribution of monoterpenes),
27 enzyme activities (pkat/mg) and terpineol/cineole ratios in the mutants F266S and F266V and
28 wildtype cineole synthase (*E.coli* crude extract) of *Nicotiana suaveolens*

	mutant F266C 1 crude extract	mutant F266C 2 crude extract	mutant F266T crude extract	mutant F266Y crude extract	wild type crude extract
	specific activity [pkat/mg]				
sabinene	0	0	0	5.5 ± 1.3[b]	1.6 ± 1.5[a]
β-myrcene	0	0.2	0	2.9 ± 0.2[b]	2.1 ± 1.5[a]
limonene	0	0.2	0	1.8 ± 0.3[b]	1.6 ± 1.2[a]
1,8-cineole	1.8	8.3	0	14.7 ± 3.5[b]	15.4 ± 11[a]
α-terpineol	1.7	3.9	1.7 ± 0.7[a]	9.5 ± 2.7[b]	6.4 ± 4.1[a]
	total specific activity [pkat/mg]				
	3.5	12.6	1.7 ± 0.7[a]	34.3 ± 8[b]	27.2 ± 18.9[a]
	α-terpineol/1,8-cineole ratio				
	1 : 1.06	**1 : 2.1**	**1 : 0**	**1 : 1.5**	**1 : 2.4**
	distribution [%]				
	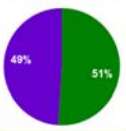	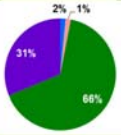		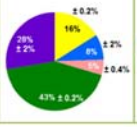	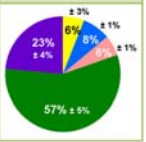

29

30 Supplemental **Figure S1G**: Analysis of volatile profiles (% distribution of monoterpenes),
31 enzyme activities (pkat/mg) and terpineol/cineole ratios in the mutants F266C, F266T, F266Y
32 and wildtype cineole synthase (*E.coli* crude extract) of *Nicotiana suaveolens*

Supplemental **Figure S2**: SDS-PAGE and Western blot of the purified wild type and mutant (F266S, F266T, F266V) enzymes of *Nicotiana suaveolens*

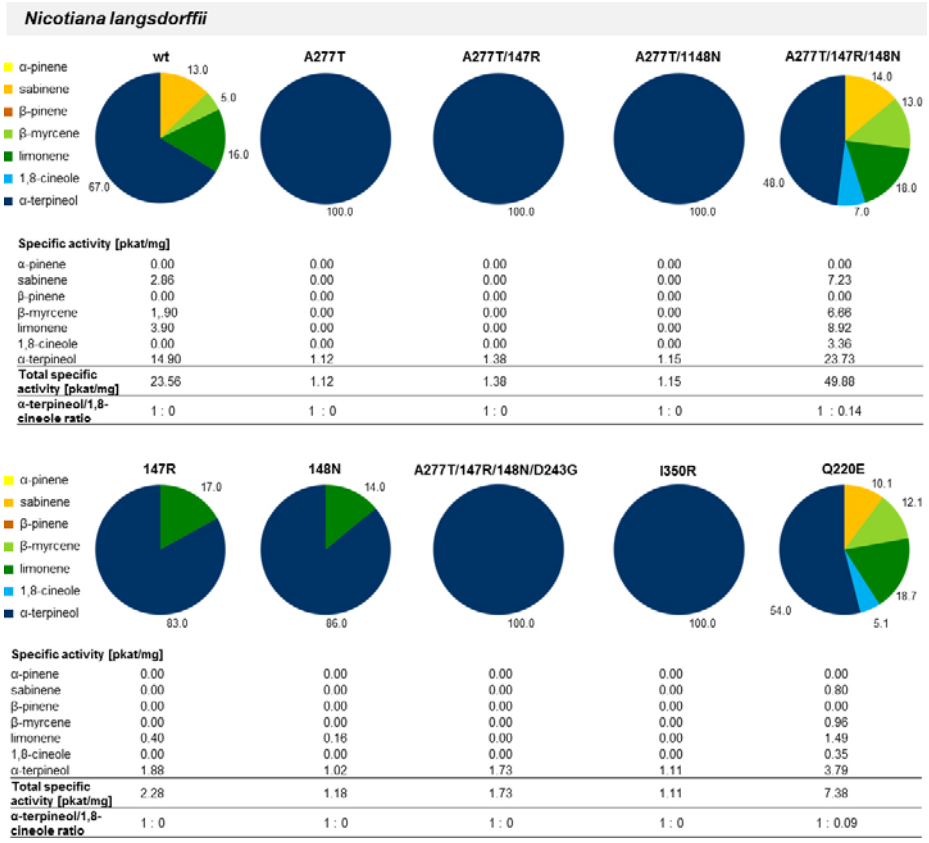

Specific activity [pkat/mg]					
α-pinene	0.00	0.00	0.00	0.00	0.00
sabinene	2.86	0.00	0.00	0.00	7.23
β-pinene	0.00	0.00	0.00	0.00	0.00
β-myrcene	1,.90	0.00	0.00	0.00	6.66
limonene	3.90	0.00	0.00	0.00	8.92
1,8-cineole	0.00	0.00	0.00	0.00	3.36
α-terpineol	14.90	1.12	1.38	1.15	23.73
Total specific activity [pkat/mg]	23.56	1.12	1.38	1.15	49.88
α-terpineol/1,8-cineole ratio	1 : 0	1 : 0	1 : 0	1 : 0	1 : 0.14

Specific activity [pkat/mg]					
α-pinene	0.00	0.00	0.00	0.00	0.00
sabinene	0.00	0.00	0.00	0.00	0.80
β-pinene	0.00	0.00	0.00	0.00	0.00
β-myrcene	0.00	0.00	0.00	0.00	0.96
limonene	0.40	0.16	0.00	0.00	1.49
1,8-cineole	0.00	0.00	0.00	0.00	0.35
α-terpineol	1.88	1.02	1.73	1.11	3.79
Total specific activity [pkat/mg]	2.28	1.18	1.73	1.11	7.38
α-terpineol/1,8-cineole ratio	1 : 0	1 : 0	1 : 0	1 : 0	1 : 0.09

Supplemental **Figure S3**: Analysis of volatile profiles (pie chart: % distribution of monoterpenes), enzyme activities (pkat/mg) and terpineol/cineole ratio of mutants of terpineol synthase (*E.coli* crude extract) of *Nicotiana langsdorffii*

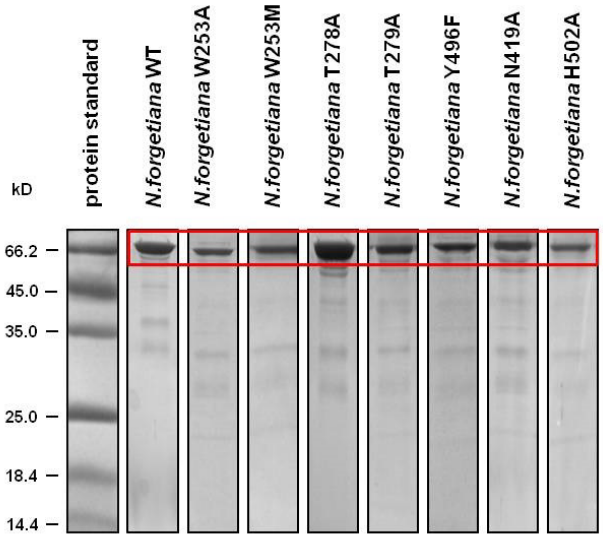

Supplemental **Figure S4**: Purification of the recombinant wild type and mutant cineole synthase of *Nicotiana forgetiana*

A

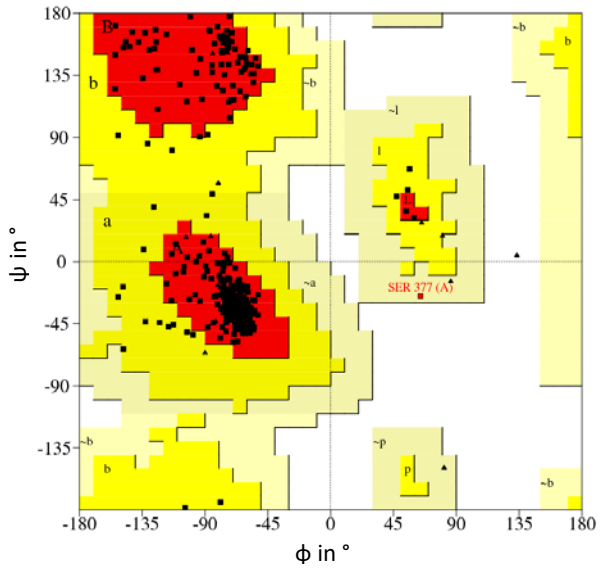

Portion of dihedrals of peptide backbone in:

most favoured region(red)
95.3%
additionally allowed region (yellow)
4.5%
generously allowed region (pale yellow)
0.2%
disallowed region (white)
0%

Planarity of peptide bonds
4.4° s.d.

B

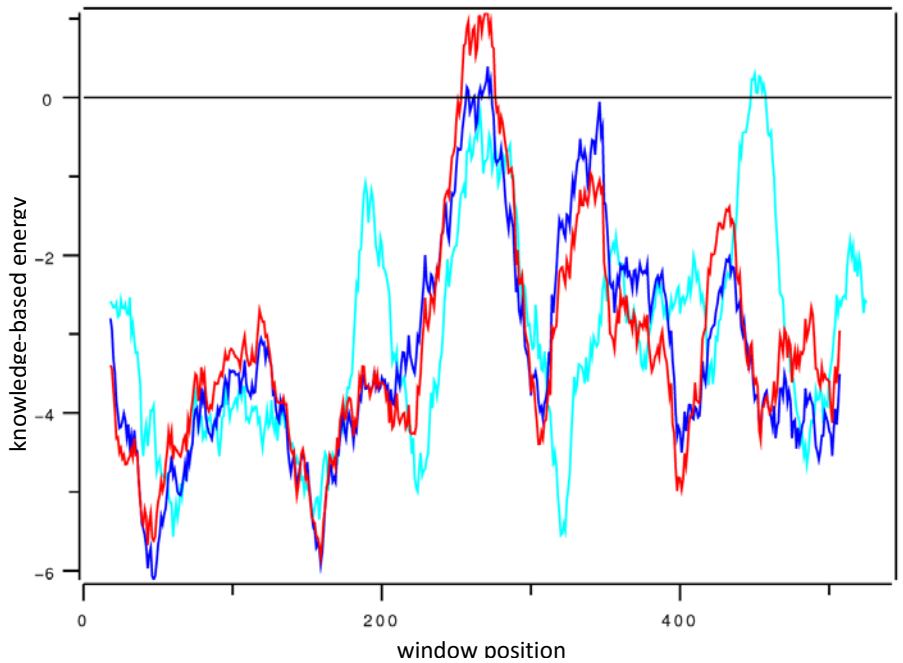

C

	PROSA Z-*score**	Q_{MEAN}**
Nicotiana forgetiana CIN after initial modelling	-12,55	0,674
Nicotiana forgetiana CIN after model refinement	-12,77	0,71
Salvia fruticosa LIM crystal structure	-13,66	0,677

*the more negative, the better **the more positive, the better

D

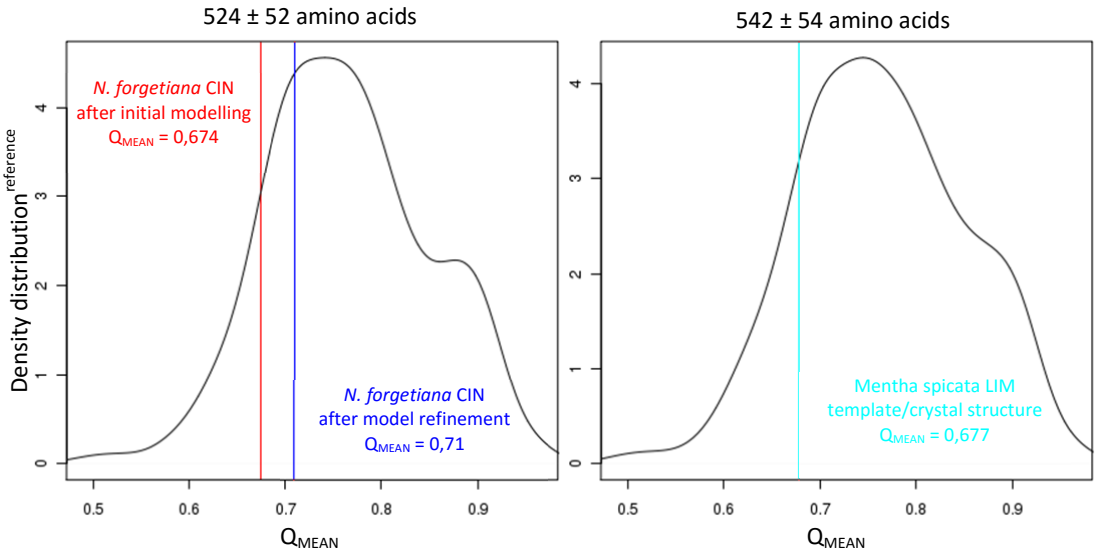

Supplemental **Figure S5A-D**: Supporting calculations for 3D model of cineole synthase of *Nicotiana forgetiana*

A) Ramachandran plot of the final model of the cineole synthase of *Nicotiana forgetiana* generated with PROCHECK (Laskowski et al 1993).

B) PROSA-*plot* of the homology model of the cineole synthase *Nicotiana forgetiana* after initial (red) modelling and refinement (blue). For comparison the main template of limonene synthase of *Mentha spicata* (2ONH) is shown (cyan).

C) Scores of model evaluation programs.

D) Comparison of QMEAN results of homology models of the cineole synthase of *N. forgetiana* and the crystal structure of the limonene synthase of *Mentha spicata* and a reference dataset provided by QMEAN (Benkert et al. 2008).

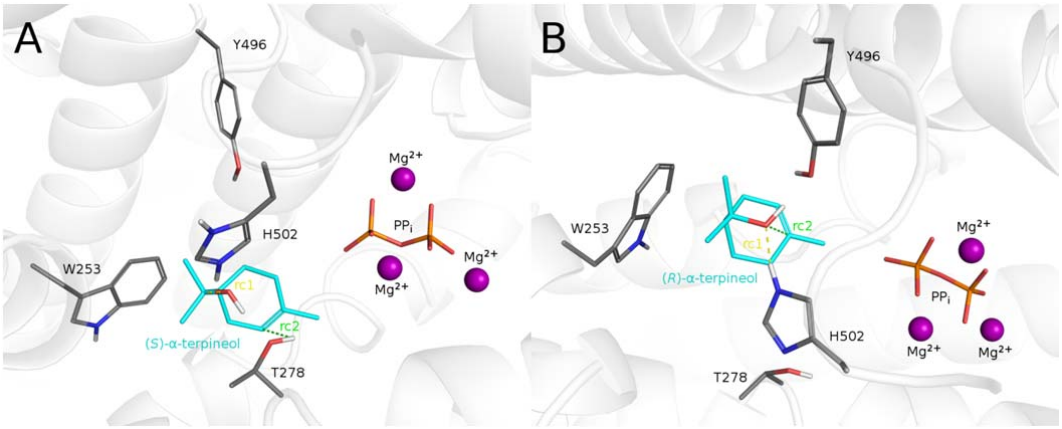

A

reaction coordinate 1 (rc1)	reaction coordinate 2 (rc2) in Å																								
	3.4	3.3	3.2	3.1	3.0	2.9	2.8	2.7	2.6	2.5	2.4	2.3	2.2	2.1	2.0	1.9	1.8	1.7	1.6	1.5	1.4	1.3	1.2	1.1
2.2	9.7	9.7	9.7	9.8	9.9	10.1	10.3	10.5	10.8	10.9	11.8	12.1	13.4	14.6	16.3	18.3	20.6	23.8	27.7	32.2	31.7	39.3	46.8	6.1
2.1	5.4	5.5	5.5	5.5	5.7	5.3	5.4	5.5	5.7	6.0	6.3	6.8	7.6	8.5	9.9	11.8	14.2	53.9	41.9	29.9	19.2	10.9	6.2	6.4
2.0	6.1	6.0	6.0	6.0	6.0	6.0	6.1	6.3	6.4	6.6	7.0	7.4	8.1	9.1	10.5	12.3	14.6	17.6	21.4	25.3	31.2	38.2	6.8	7.0
1.9	6.5	6.4	6.3	6.3	6.7	6.7	6.7	6.8	6.8	6.5	6.8	7.1	7.9	8.7	9.9	11.6	13.8	54.6	43.1	31.2	20.5	12.1	7.4	7.7
1.8	6.1	6.0	5.9	5.8	5.4	5.4	5.4	5.5	5.6	5.8	6.4	6.9	7.1	8.1	9.4	11.1	13.3	15.9	19.8	24.3	29.6	35.6	7.8	8.1
1.7	4.1	3.9	3.7	3.6	3.5	3.4	3.5	3.6	4.6	4.8	5.1	6.2	6.7	7.6	8.8	10.3	12.5	54.1	43.5	31.6	20.9	12.6	7.9	8.2
1.6	2.7	2.4	2.2	2.0	1.8	1.7	1.7	1.6	1.7	1.9	2.2	2.7	3.6	4.8	6.4	8.4	10.8	13.7	17.1	21.1	26.0	11.2	6.7	7.1
1.5	1.5	1.2	1.1	0.7	0.4	0.2	0.0	-0.1	-0.1	0.0	0.6	1.2	2.1	2.9	5.3	7.1	9.4	51.5	39.1	27.2	**16.8**	**8.5**	**3.8**	**4.0**
1.4	**0.0**	**-0.4**	**-0.8**	**-1.2**	**-1.8**	**-2.2**	**-2.5**	**-2.7**	**-2.9**	**-2.9**	**-2.7**	**-2.3**	**-1.7**	**-0.6**	**0.8**	**2.7**	**5.0**	**8.0**	**11.8**	**16.6**	22.6	29.9	14.8	15.4
1.3	5.6	5.2	4.7	4.1	3.6	3.3	3.1	2.9	2.8	2.9	3.1	3.5	4.2	5.2	6.6	8.4	10.6	13.5	26.4	27.8	28.7	22.5	19.4	20.6

rc1 = C7, terpineol ↔ O7, terpineol; rc2 = C2, terpineol ↔ HG1, Thr278

B

coordin	reaction coordinate 2 (rc2) in Å																					
	3.1	3.0	2.9	2.8	2.7	2.6	2.5	2.4	2.3	2.2	2.1	2.0	1.9	1.8	1.7	1.6	1.5	1.4	1.3	1.2
1.8	**0**	**0.1**	**0.3**	**0.7**	**1.4**	**2.2**	**3.4**	**5.1**	**7.2**	**10.2**	**14.0**	**18.9**	20.0	13.5	**7.0**	**0.6**	**-4.3**	**-5.2**	1.1	20.4
1.7	0.2	0.2	0.5	0.9	1.5	2.4	3.6	5.2	7.4	10.4	14.2	19.2	**19.8**	**13.3**	7.1	1.0	-3.8	-4.6	1.8	21.2
1.6	0.7	0.8	1.0	1.5	2.1	3.0	4.2	5.8	8.0	11.1	14.9	19.8	19.7	13.1	7.4	1.7	-2.8	-3.5	3.1	22.7
1.5	1.9	2.0	2.2	2.7	3.3	4.2	5.4	7.0	9.2	12.3	16.0	21.2	20.1	14.2	8.5	3.3	-1.1	-1.8	5.0	25.0

	1.4	4.1	4.2	4.4	4.8	5.4	6.4	7.5	9.0	11.2	14.2	18.2	23.2	19.4	15.2	9.7	4.3	0.3	0.2	7.7	28.3
	1.3	7.7	7.9	8.0	8.3	8.9	9.9	10.9	12.5	14.6	17.3	21.3	24.3	20.7	15.6	11.0	6.9	4.0	4.8	12.7	32.7
	1.2	12.3	12.2	12.3	12.8	13.3	13.9	15.1	16.3	18.3	21.0	24.9	24.5	21.7	18.1	14.5	10.4	7.4	8.3	16.7	38.3
	1.1	17.4	17.5	17.4	17.7	18.0	18.7	19.7	21.0	21.7	24.4	26.1	24.2	22.0	19.4	16.2	12.9	11.8	13.6	22.8	45.0

rc1 = HE2, His502 ↔ O7, terpineol; rc2 = C3, terpineol ↔ O7, terpineol

Supplemental **Figure S6**: MOPAC grid calculations to examine the energy barriers of the reaction path from α-terpineol to 1,8-cineole of *Nicotiana forgetiana*

Reaction coordinates are marked in yellow and green, respectively, and differ between (*R*)- and (*S*)-α-terpineol (A: (*S*)-α-terpineol, B) (*R*)-α-terpineol). Interestingly, the starting geometries differ considerably. Energies in tables are presented relative to the energy of the starting geometry of the putative reaction path (in kcal/mol).

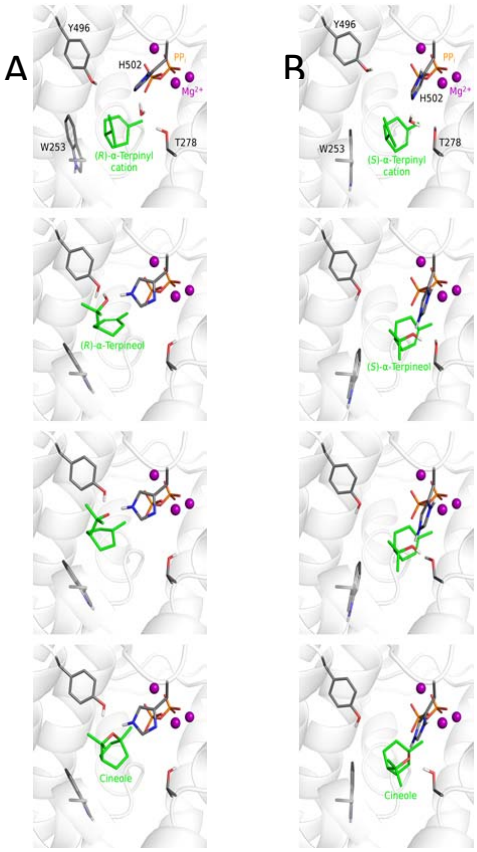

Supplemental **Figure S7**: Reaction path from α-terpinyl cation to 1,8 cineole in *Nicotiana forgetiana*

Proposed reaction path considering the *R* stereoisomer (A) and the *S* stereoisomer (B)